MORPHOLOGICAL AND MECHANICAL CHARACTERIZATION OF REINFORCEMENT IN CRACKED ELEMENTS EXPOSED TO CHLORIDE-INDUCED CORROSION

Bruno Leporace-Guimil, Nicoletta Russo, Federica Lollini and Antonio Conforti

Bruno Leporace-Guimil
Ph.D., Postdoctoral fellow
Civil and Environmental Engineering Department, Universitat Politècnica de Catalunya, Spain
Tel: +34 93 401 77 49
bruno.leporace@upc.edu

Nicoletta Russo

Ph.D. Postdoctoral fellow

Department of Chemistry, Materials and Chemical Engineering "Giulio Natta", Politecnico di Milano, Italy

Tel: +39 0223994732
nicoletta.russo@polimi.it

Federica Lollini

Ph.D. Associate Professor of Material Science and Technology

Department of Chemistry, Materials and Chemical Engineering "Giulio Natta", Politecnico di Milano, Italy

Tel: +39 0223993144
federica.lollini@polimi.it

Antonio Conforti
Ph.D., Associate Professor of Structural Engineering

Department of Civil, Environmental, Architectural Engineering and Mathematics (DICATAM)
University of Brescia, Italy
Tel: +39 0303711286; Fax: +39 0303711312
antonio.conforti@unibs.it

ABSTRACT

In Reinforced Concrete (RC) structures exposed to chloride-bearing environments, reinforcement corrosion might be initiated (preferentially occurring at crack location). A deep knowledge on the correlation between the mechanical properties of corroded bars and corrosive attack morphology, useful for the evaluation of the residual bearing capacity of structure, is still lacking. In this paper, morphological and mechanical characterization of steel reinforcement embedded in RC specimens (with and without fibers) both in cracked stage and subjected to cyclic exposure to a 5% NaCl solution for 280 days was carried out. Although a chloride content higher than the critical chloride threshold was also measured in correspondence of uncracked concrete, corrosive attacks were observed only in correspondence of cracks. Pits were mostly characterized by a shallow morphology, which led to a rebar diameter loss ranging between 1 to 10%. Furthermore, the results showed that both yielding and ultimate load of corroded rebars can be predicted by combining circular residual cross-section and mechanical properties of uncorroded rebars.

Keywords: chloride-induced corrosion; cracks; chloride content; diameter loss; pit morphological characterization; mechanical properties.

LIST OF SYMBOLS

ϕ_0	bar diameter
ϕ_f	residual bar diameter at the minimum cross-section
$\Delta\phi$	diameter loss
A_0	cross-sectional area of reinforcement
c	concrete cover
CC	critical crack
CMOD	crack mouth opening displacement
d_{pit}	pit depth at the minimum cross-section
f_c	mean value of the cylinder compressive concrete strength
$f_{R,1}$	mean value of residual flexural tensile strength corresponding to CMOD = 0.5 mm
$f_{R,3}$	mean value of residual flexural tensile strength corresponding to CMOD = 2.5 mm
F_u	ultimate load of reinforcement
f_u	ultimate strength of reinforcement
$F_{u,th}$	predicted ultimate strength of reinforcement
F_y	load at yielding of reinforcement
f_y	yield strength of reinforcement
$F_{y,th}$	predicted yielding strength of reinforcement
l_{pit}	pit length at the minimum cross-section
s_r	mean crack spacing
v_{corr}	mean pitting corrosion rate
w	means crack width
w_{pit}	pit width at the minimum cross-section
ε_u	ultimate strain of reinforcement
ε_y	yield strain of reinforcement

ΔCl Chloride content increment along the rebar due to the presence of cracks

$Cl_{\perp cr,x}$ Chloride concentration at the depth x in the direction perpendicular to crack wall

$Cl_{uncr,4}$ Chloride content at rebar depth (about 41 mm) in uncracked conditions

1. INTRODUCTION

Chloride-induced corrosion of steel rebars is one of the most detrimental phenomena affecting Reinforced Concrete (RC) structures worldwide [1]. Under these exposure conditions, the service life in the design stage is usually considered to coincide with corrosion initiation time, which is the time needed for chlorides to reach the steel surface in a sufficient amount to cause corrosion initiation. Nevertheless, in RC structures exposed to chloride-rich environment, corrosion might be initiated. Furthermore, in RC structures the presence of cracks could significantly change the aleatory nature of corrosion initiation on steel reinforcement. In fact, studies in the literature concerning the penetration of chlorides in concrete without reinforcement, seem to agree, in general, that cracks decrease the resistance to chloride penetration, and consequently, may reduce the initiation time [2]. This effect is confirmed by the available literature on RC specimens in cracked stage, even if it is not clear to which extent, and how the geometrical features of cracks (mainly crack width is considered) are involved [3]. The crack depth seems to also have an influence in reducing corrosion initiation time [4].

Cracks may also affect the corrosion propagation phase, even if this aspect is still under investigation. Jaffer and Hansson, Otieno et al., and Wang et al. found that cracks reduced the corrosion initiation time and increased the corrosion rate during the propagation stage [5–7]. However, the increase in corrosion rate is still controversial since it was observed to be more marked for short exposure times, but the effect of cracks may decrease with time [3,6]. Moreover, also crack width could play a role, in this respect. It was hypothesized that for smaller crack widths (0.1 mm or lower) either self-healing of cracks or the accumulation of corrosion products in the crack led to a slowdown of corrosion propagation due to oxygen deficiency [8].

The presence of corrosive attacks, that in a RC element in cracked stage could preferentially initiate in correspondence of cracks [9], has consequences on the mechanical behavior of steel reinforcement and therefore on the bearing capacity and ductility of the whole structure. Chloride-induced corrosion process involves a localized corrosive attack (pit) that reduces locally the resistant cross-section of the rebar. This leads to a reduction of both ultimate load and strain of rebars [10–12], even though the ultimate strain is the more affected parameter. Pitting corrosion seems not to reduce the ultimate strength (f_u) of rebars [10, 12, 13], even if its calculation is complicated due to the uncertainties in evaluating the residual cross-section. The stiffness of rebars in tension and the bond between rebars and concrete can be also influenced by pitting corrosion. Few studies, anyway, correlate the mechanical properties of corroded rebar to a characterization of pit morphology [10,13–15]. In some studies, pits are reproduced with a controlled process by mechanically removing part of the resistant cross-section [14,16,17]. In other cases, accelerated corrosion is performed to speed up the corrosive process, for example by means of an externally applied current [13,18–23]. These procedures can anyway be not fully representative of the electrochemical processes and corrosion morphology that occur in real RC structures. Corrosion induced by the simple exposure to chlorides and propagated naturally was considered in few studies and among these, very few were carried out on RC elements that were exposed to chlorides under loading [6,11,24,25], therefore considering crack widths and morphology representative of service life conditions in real structures.

Finally, another aspect to be considered is the microstructure of steel reinforcement. Rebars produced by a quench and self-tempering process (TEMPCORE^{TM}) are generally used in RC structures. The mechanical and ductility behavior of corroded TEMPCORE bars also depends on which layer is affected by pitting corrosion since the microstructure on the rebar cross-section is not uniform [26]. In particular, the martensitic outer annulus is characterized by higher strength and lower ultimate strain as compared to the inner core, as clearly shown in Haefliger et al. [17]. In addition, the depth of the corrosion attack seems to be related to the microstructures of TEMPCORE bars as proved by Bautista et al. [26].

There is therefore an increasing need for the assessment of the morphology of corrosive attacks naturally propagated in RC elements under service life conditions, and their effect on the mechanical behavior of steel reinforcement. A further interest, moreover, is related to the use of steel fibers technology to better control cracking under loading, and the effectiveness in reducing reinforcement corrosion [11,24]. A better understanding of these mechanisms could give useful information on how to perform the capacity and ductility assessment of RC elements with and without fibers affected by corrosion.

In this study, morphological and mechanical characterization of corrosive attacks was performed on steel reinforcement embedded in RC and Steel Fiber Reinforced Concrete (SFRC) specimens in cracked stage, subjected to serviceability loading conditions. These specimens came from a previous study in which the exposure to chlorides lasted for 280 days and rebar corrosion initiation and propagation occurred naturally. At the end of the exposure, the rebar was extracted from the specimens and cleaned, the corrosive attacks were observed, and a tensile test was performed on the whole rebar Leporace-Guimil et al. [11]. Subsequently, it was decided to implement other analyses to further characterize the pits and their effect on the mechanical response of steel rebars. In particular, the morphological characterization of corrosive attacks was performed (considering also the microstructural layers of the steel rebar) and chloride analyses were carried out in correspondence with cracks and uncracked concrete to better understand the effects of cracks on corrosion initiation and propagation processes. Finally, a uniaxial tensile test was performed on different segments of rebar including one single pit, to evaluate the influence of the pits and their morphology on the tensile behavior of steel rebars.

2. MATERIALS AND SPECIMEN GEOMETRY

2.1 Description of specimens

Hot-rolled ribbed TEMPCORE bars of grade B500B with a nominal diameter (ϕ_0) of 12 mm extracted from prismatic concrete specimens (830 mm long with a square cross-section having a side length of 90 mm, Figure 1) were analyzed in this study. Rebars were characterized by f_y and f_u equal to 599 MPa (CV = 0.01) and 696 MPa (CV=0.01), while yield (ε_y) and ultimate strain (ε_u) were equal to 0.3% (CV = 0.06) and 8.6% (CV = 0.08), respectively. Each rebar (used "as received" from the steel manufacturer) was placed along the concrete specimen axis, leading to a concrete cover equal to 39 mm. Five specimens were made in ordinary concrete (RC) and five with steel fiber reinforced concrete with 50 kg/m^3 of steel fibers (SFRC50), in both cases with a water/cement ratio of 0.5. Cylinder compressive concrete strength was of about 38 MPa. Specimens were firstly pre-cracked applying a tensile load up to 34 kN (which correspond to a stress on rebar equal to 300 MPa and crack width between 0.1 to 0.2 mm, which are typical values occurring in RC structures at serviceability limit states) by using and INSTRON machine. Secondly, specimens were subjected to chloride-induced corrosion. During the exposure period to chlorides, specimens were kept under a constant tensile load of 34 kN (to maintain specimens in a cracked stage representative of service conditions in real structures) and they were subjected to wet-dry weekly cycles in a water solution containing 5% of NaCl for 280 days (Figure 1). Threaded bars with strain gauges were used to connect the specimens to the self-equilibrating steel frame (Figure 1) and to measure continuously the load during the exposure period. No impressed current technique was adopted. The dry condition occurred in an environment with a temperature of 20 ± 2 °C and relative humidity of 55 ± 5%. At the applied constant tensile load, the mean crack width resulted in 0.189 mm (with a mean crack spacing of about 170 mm) and 0.119 mm (with a mean crack spacing of about 143 mm) for RC and SFRC50 specimens, respectively. Thus, all samples were characterized by at least

4-5 cracks. No corrosion-induced cracks were observed. More details about materials, specimen geometry, and corrosion procedure can be found in Leporace-Guimil et al. [11].

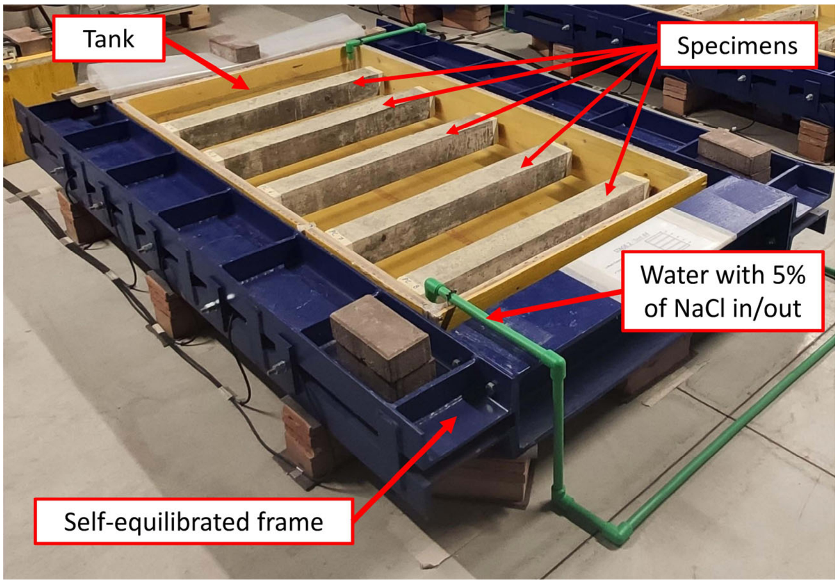

Figure 1: Specimens exposed to wet-dry cycles with chloride solution while kept under constant tensile load in a self-equilibrated frame.

At the end of exposure, reinforcement bars were extracted by dry cutting the specimens in two halves along the rebar direction with a saw. After being extracted from concrete specimens, rebars were cleaned by metallic bristle brushing and carefully studied. Analyses in terms of weight loss, the influence of steel fibers, and relationships between pit depth/length of corrosion zone and crack width were carried out and results were already published in Leporace-Guimil et al. [11]. Subsequently, for three specimens per each concrete type, further studies were carried out to better understand the corrosion attacks and their effects on the reinforcement mechanical properties. Particular attention was devoted to the pit morphology (Section 2.2), chloride content in concrete around rebars (Section 2.3), and to the influence of pitting corrosion on the mechanical properties of rebars. The latter was experimentally evaluated by testing, under uniaxial tension, segments, longer than 300 mm, cut out from rebars extracted from concrete specimens, containing the pit almost in the central position. These tests were carried out by using an Instron Machine equipped with a biaxial extensometer 50 mm axial gauge length. The influence of the gauge length on the measured ultimate strain of corroded rebars can be found in [10]. In fact, the ultimate strain seems to be strongly affected by the adopted gauge length [10].

2.2 Characterization of pit morphology

After cleaning the rebars, the local damage due to corrosion on rebars was evaluated by using a dial indicator 0.001 mm reading and a digital microscope (1.3 Megapixel resolution and 10- 70x and 200x magnification). The dial indicator was used in correspondence of each crack to identify the location of the minimum remaining cross-section and the related maximum pit depth (d_{pit}, Figure 2a). Then, pit width (w_{pit}, Figure 2a) and maximum pit length (l_{pit}) were obtained by analyzing the images captured by the digital microscope. Other pits present at the crack location were detected by following the same procedure adopted for the minimum remaining cross-section as well.

Based on these measurements, the residual cross-section was calculated, characterized by a residual bar diameter ϕ_f, as reported in Figure 2a. This residual cross-section was evaluated by assuming the loss in diameter ($\Delta\phi$) and not the loss in section. In particular, ϕ_f and $\Delta\phi$ were calculated as follows:

$$\phi_f = \phi_0 - d_{pit} \quad (1)$$

$$\Delta\phi = \frac{d_{pit}}{\phi_0} \quad (2)$$

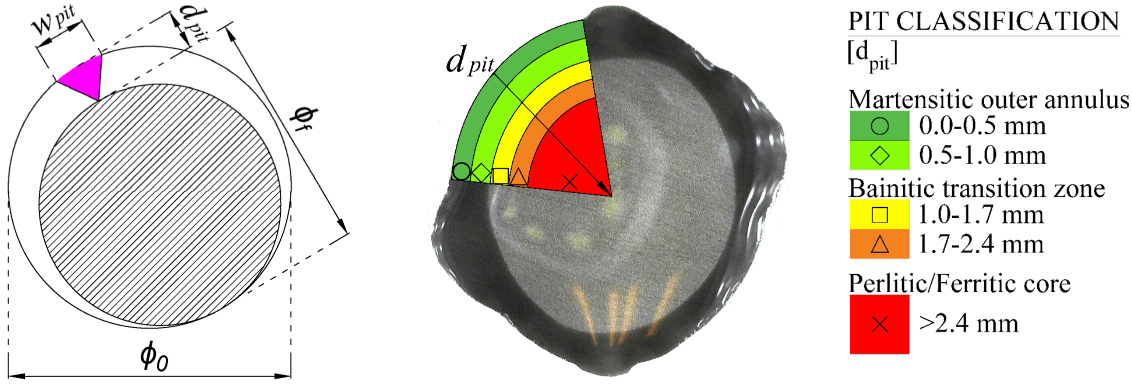

(a) (b)

Figure 2: Residual cross-section (hatched area) considering the loss in diameter (a); layers in Ø12 rebars and pit classification as a function of both d_{pit} and compromised layer (b).

Additionally, the martensitic outer annulus of the rebar under investigation was evaluated by microscope on the surface of cut samples previously treated by polishing and edging (by Nital 3%). The martensitic outer annulus is clearly visible (dark gray part) in Figure 2b. It was not possible to identify the bainitic transition zone by using this methodology, and thus, it was estimated according to the values collected in Haefliger and Kaufmann [17]. The different microstructural layers were identified in order to propose a pit classification as a function of both d_{pit} and compromised layer (Figure 2b).

2.3 Chloride content analysis

Chloride content was estimated by sampling concrete powders and performing a potentiometric titration. Powders were dry drilled with a column drilling machine (Figure 3) and, for SFRC50 specimens, steel fibers were removed with a magnet. Powders were collected with a Ø12 drill bit until a depth of 10 mm, to obtain around 3 grams of powder per sample. The sampling of powders was performed in selected specimens after rebar removal. In particular, powders were collected on one of the two halves of the specimens, considering one portion included between two different cracks, as illustrated in Figure 3. Chloride profiles were obtained for each concrete portion from the analysis of five different sets of powders, that were determined considering the symmetry of the specimen, and considering that chlorides penetrated from all the lateral surfaces. As shown in Figure 3c, the sets of powders were drilled:

- in the uncracked zone, approximately in a central position between the 2 cracks (3 holes from the exposed surface towards rebar depth, and 3, that will then be averaged, at rebar depth);
- in correspondence of each crack, at rebar depth, from the crack wall towards the uncracked zone (perpendicular to the crack wall, 4 holes);
- for each crack in correspondence to the crack wall (direction parallel to crack, 4 holes from the exposed surface until rebar depth, with the last sample in common to the profiles perpendicular to crack wall).

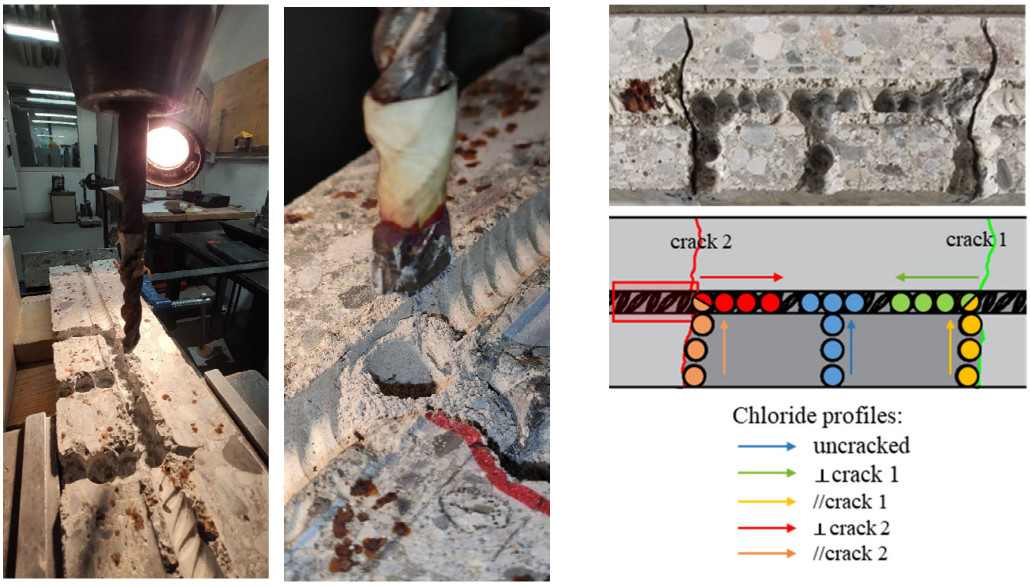

(a) (b) (c)

Figure 3: Powder sampling by column drilling machine for the evaluation of the chloride content (a,b); chloride profiles in uncracked concrete (blue), perpendicular to crack wall (red and green) and parallel to crack wall (orange and yellow) (c).

After sampling, powders were dried in an oven at 105°C for at least 24 hours, weighted to obtain the dry mass, and dissolved in a boiling nitric acid solution. Potentiometric titration was then performed with an automatic potentiometric titrator, model Mettler Toledo Easy Plus Titration.

3. RESULTS AND DISCUSSION

3.1 Morphological characterization of pitting corrosion

For a complete overview of the analyzed specimens, Figure 4 and Figure 5 show a schematic representation of the RC and SFRC50 specimens, respectively, including crack pattern and average crack width, pictures of the pits, and pit morphology classification according to the compromised layer (symbols recalling Figure 2b). Moreover, zones affected by corrosive attacks are highlighted with red squared areas, while the powder samplings for chloride profiles are represented with red circles.

Corrosion pits were only observed in correspondence of cracks in both RC and SFRC50 specimens, while no corrosion was observed in correspondence of uncracked concrete. Nevertheless, in few cases, no pits were found even in correspondence of cracks. This occurred twice in RC specimens, in correspondence of cracks with an average width of 0.185 mm and 0.179 mm, while just once in an SFRC50 specimen, where the crack had an average width of 0.065 mm. In correspondence to some cracks, more than one pit was observed (in these cases each pit was labeled with a letter).

Table 1 summarizes the morphological characteristics of the corrosion pits in correspondence with the minimum remaining cross-section around cracks. For each pit, the dimensions in terms of depth (d_{pit}), width (w_{pit}), and length (l_{pit}) are reported, and according to pit depth, Table 1 reports also which layer of the steel rebar was compromised by corrosion and the diameter loss ($\Delta\phi$), calculated according to Equation 2.

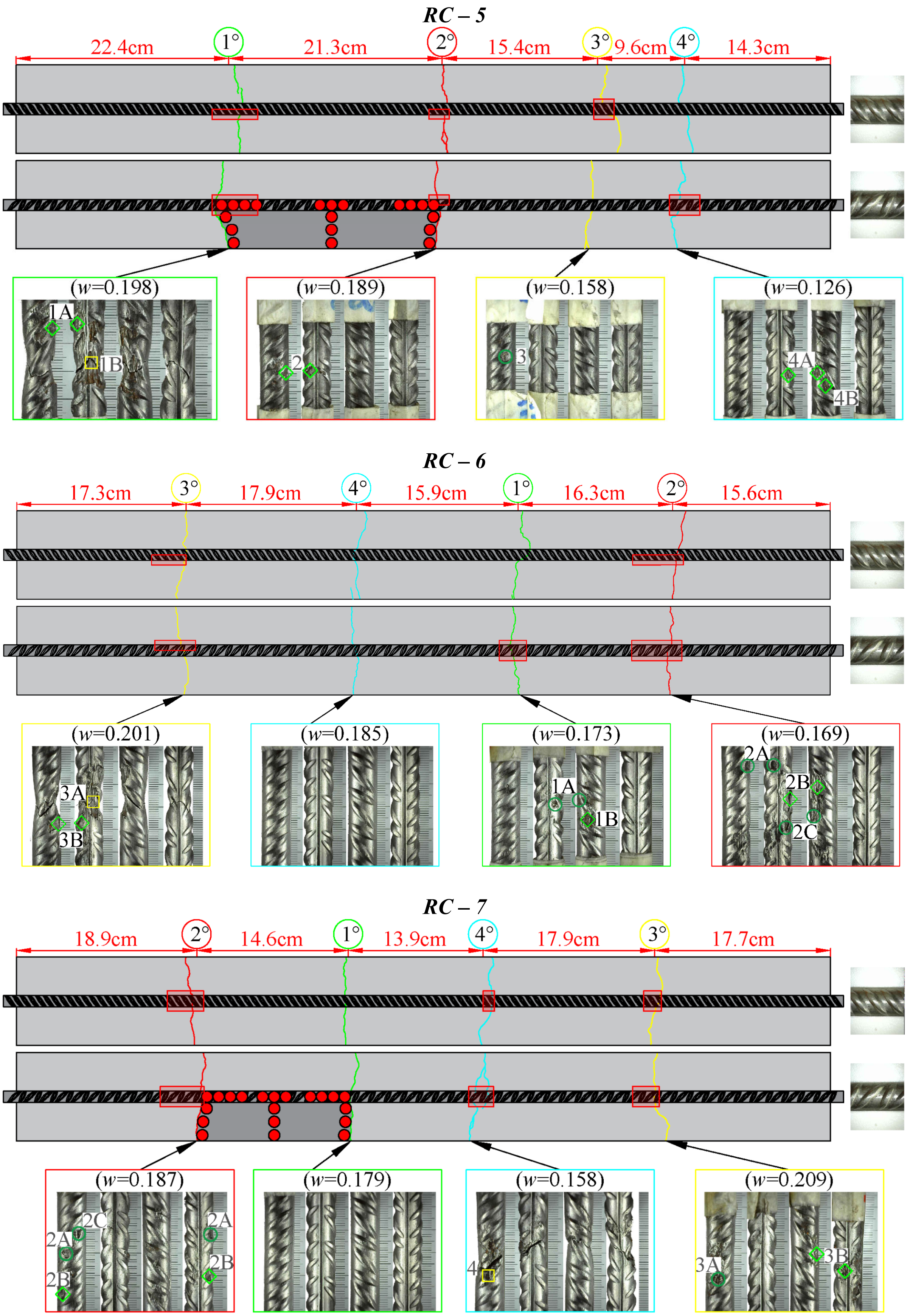

Figure 4: Schematic drawing of RC specimens with crack pattern, areas where corrosion was observed (red squares), powder sampling for chlorides (red circles), and pit classification.

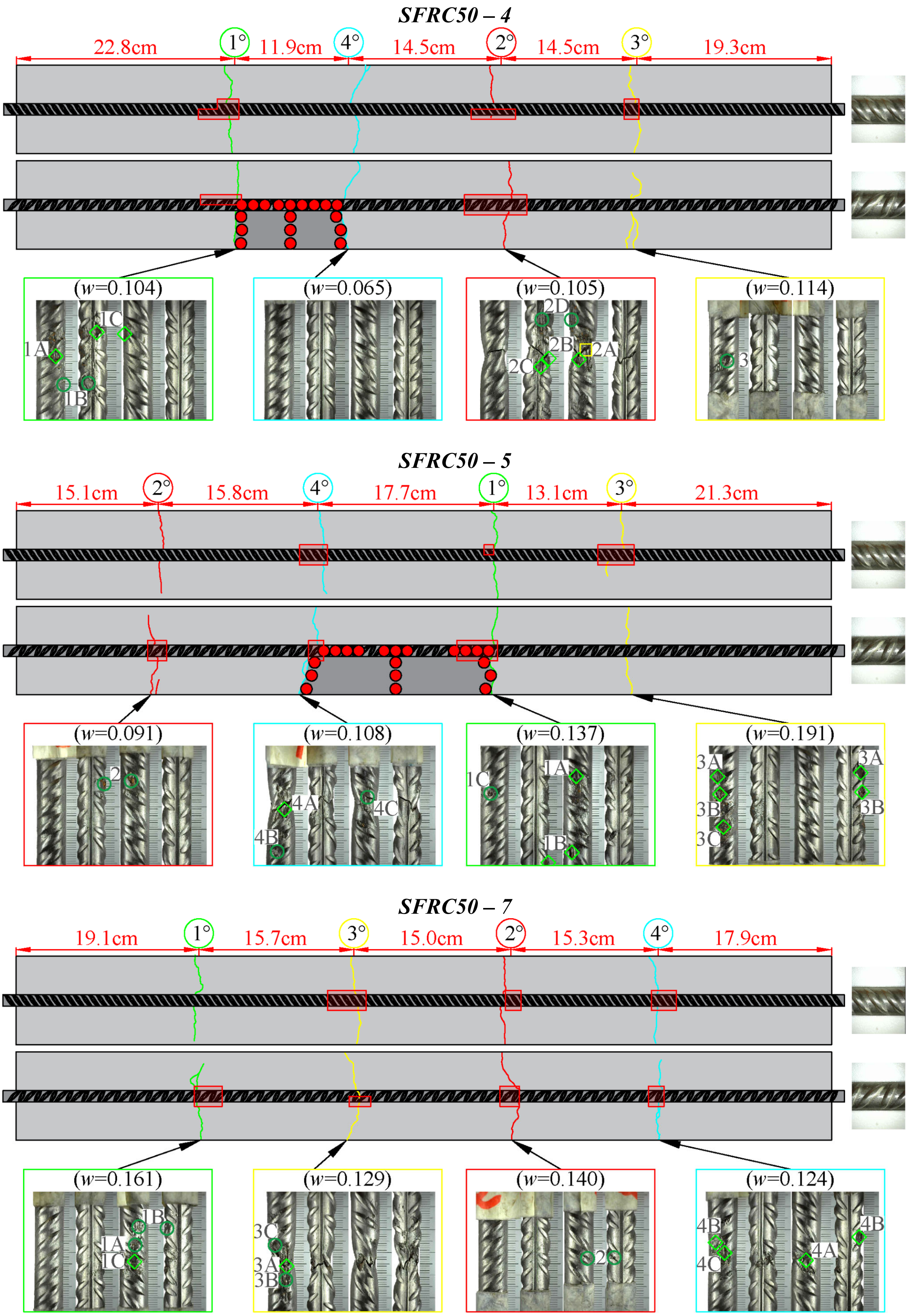

Figure 5: Schematic drawing of SFRC50 specimens with crack pattern, areas where corrosion was observed (red squares), powder sampling for chlorides (red circles) and pit classification.

Table 1: Morphological characteristics of main pits in correspondence of the minimum remaining cross-section around cracks.

Specimen	Crack n°	Pit label	d_{pit} [mm]	w_{pit} [mm]	l_{pit} [mm]	Compromised layer	Diameter loss $\Delta\phi$ [%]
RC-5	1	B	1.005	3.590	6.134	Bainite	8.37
RC-5	2	-	0.629	9.280	4.097	Martensite	5.24
RC-5	3	-	0.135	1.077	2.763	Martensite	1.13
RC-5	4	B	0.790	3.968	3.181	Martensite	6.58
RC-6	1	B	0.618	3.796	6.194	Martensite	5.15
RC-6	2	B	0.714	2.603	7.212	Martensite	5.95
RC-6	3	A	1.238	3.436	8.622	Bainite	10.32
RC-6	4	x	x	x	x	x	x
RC-7	1	x	x	x	x	x	x
RC-7	2	B	0.658	3.521	4.314	Martensite	5.48
RC-7	3	B	0.549	2.964	4.120	Martensite	4.58
RC-7	4	-	1.143	2.936	3.455	Bainite	9.53
SFRC50-4	1	C	0.530	3.671	4.275	Martensite	4.42
SFRC50-4	2	A	1.107	4.570	7.773	Bainite	9.22
SFRC50-4	3	-	0.218	1.857	3.811	Martensite	1.82
SFRC50-4	4	x	x	x	x	x	x
SFRC50-5	1	B	0.587	2.795	4.337	Martensite	4.89
SFRC50-5	2	-	0.322	3.094	4.529	Martensite	2.68
SFRC50-5	3	C	0.664	4.498	4.970	Martensite	5.53
SFRC50-5	4	A	0.820	7.118	5.007	Martensite	6.83
SFRC50-7	1	C	0.928	3.909	2.840	Martensite	7.73
SFRC50-7	2	-	0.281	1.202	1.257	Martensite	2.34
SFRC50-7	3	A	0.827	4.491	5.310	Martensite	7.35
SFRC50-7	4	A	0.653	2.691	4.792	Martensite	5.44

x = no corrosion was detected.

Pits presented on average a quite shallow morphology, being on average 0.75 mm deep, 3.7 mm wide, and 5 mm long in RC specimens, 0.63 mm deep 3.6 mm wide and 4.4 mm long in SFRC50 specimens. Indeed, almost all the observed pits involved just the martensitic outer annulus, while in few cases developed until the bainitic transition zone, mostly in RC specimens and not necessarily in correspondence of the widest cracks. In all the cases considered, it was found that the cracks in correspondence of no corrosion were adjacent to those cracks where the deepest pits, involving the bainitic transition zone, were detected. No cases were observed in which the pearlitic/ferritic core was compromised.

The diameter loss ($\Delta\phi$) resulted included in the range 1%−10% for both the concrete types, being on average one percentage point higher for RC specimens as compared to SFRC50 specimens, 6.2% and 5.3% respectively.

3.2 Evaluation of chloride content

Figure 6 shows the chloride profiles, grouped considering the position and the direction of powder sampling, *i.e.* in uncracked concrete (Figure 6a), perpendicular to crack walls (Figure 6b), and parallel to crack walls (Figure 6c). In chloride profiles evaluated in the uncracked zone (Figure 6a), as expected, no difference was observed between RC and SFRC50 specimens, with chloride profiles having a decreasing trend from the exposed surface towards deeper layers. In correspondence to the exposed surface, chloride concentration was roughly in the range of 1.5−3.5% vs cem mass, while in the deepest layer (corresponding to the concrete cover depth, *i.e.* the position of the rebar) it was about 1%. Therefore, in both RC and SFRC50 specimens, the chloride content at the depth of the rebar was always found to be higher than the critical chloride threshold that causes corrosion initiation in carbon steel rebar, considered to be in the range of 0.4-1% vs cem mass, even if corrosion was never observed in these areas.

In the direction perpendicular to crack walls (Figure 6b), a variable chloride concentration was found in the outer layer, included in the range of 1.8-3.4% vs cem mass for RC specimens and 1.2-2.7% vs cem mass for SFRC50 specimens, comparable to those found at the exposed surface in sound conditions. For the deeper layers, chloride profiles show a quite high homogeneity in trend and a lower amount of chlorides in SFRC50 specimens with respect to RC ones. This is due to the increment of bond strength between rebar and concrete provided by fibers, as already proved by Metelli et al. [27]. This also leads to more uniform bond stresses in fiber reinforced concrete elements as compared to RC ones [27] and eventually to a lower ingress of chlorides from the crack wall. Nevertheless, the trend of all the chloride profiles was similar to that of the uncracked zones, as if the crack wall behaved as a newly exposed surface.

Again, the chloride concentration in the outer layer and almost in all the other depths was higher than the critical chloride threshold, even if in some cases no corrosion was observed in correspondence of the crack (w=0.179 mm for RC and w=0.065 mm for SFRC50).

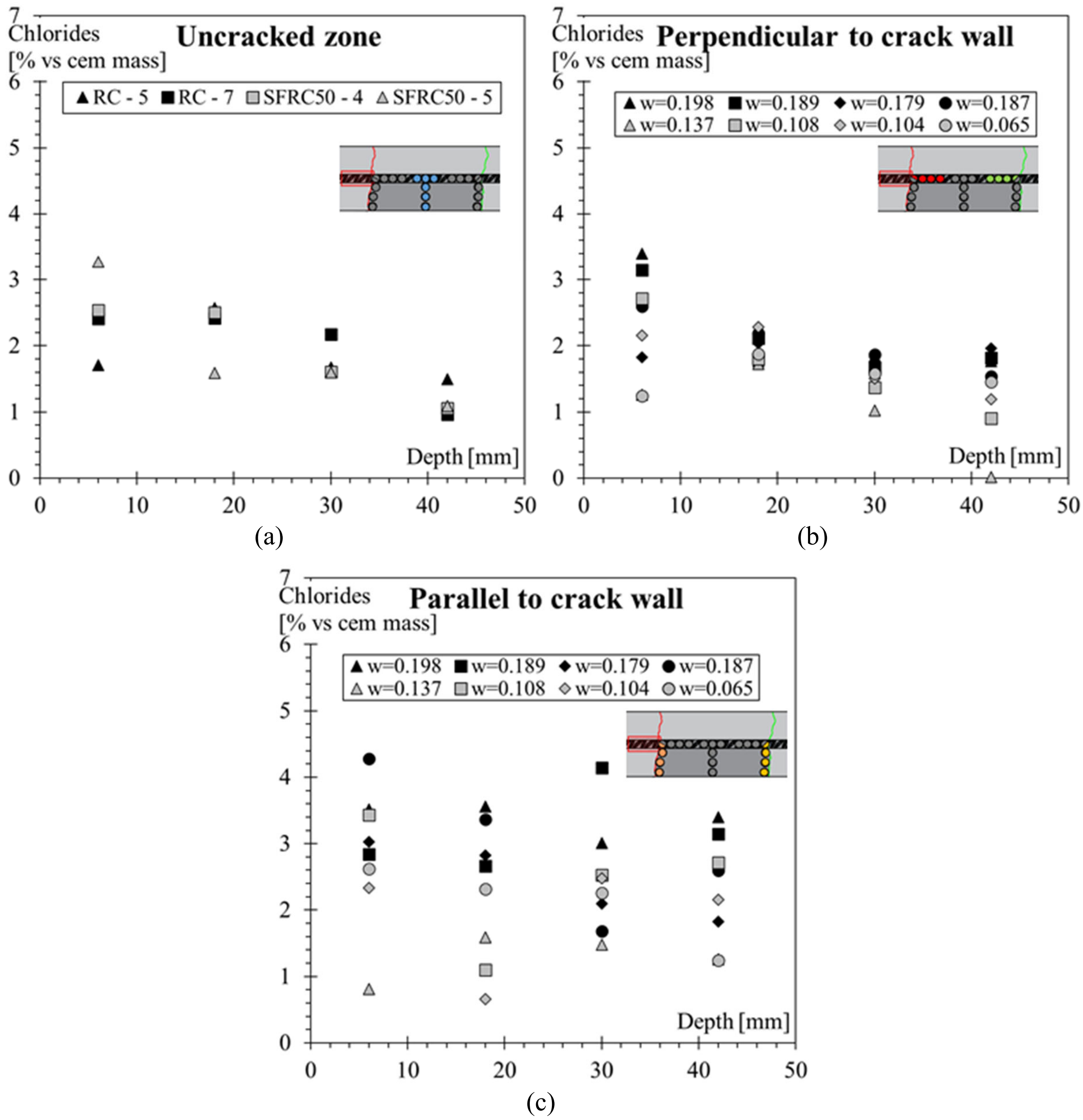

Figure 6: Chloride content vs depth in the uncracked part of the specimen (a), in the direction perpendicular (b) and parallel (c) to crack wall; black and grey symbols for RC and SFRC50, respectively, and crack width (w) in mm.

The chloride profiles in the parallel direction to crack walls (Figure 6c) show a much higher heterogeneity and variability. Chloride concentration is not decreasing as a function of depth, and variable values included in the range of 1.7−4.3% vs cem mass for RC and 0.7−3.4% vs cem mass for SFRC50 were found. No clear correlation was found between crack widths and chloride profiles, except that chloride concentration was on average lower along cracks in SFRC50 specimens, which showed on average lower crack widths. The high variability of chloride concentrations is quite representative of chloride concentration in correspondence to the exposed surface in RC structures subject to cyclic wet/dry exposure to chlorides, due to evaporation of water and redistribution of chlorides.

To better discuss the influence of the presence of the crack on the penetration of chlorides, Figure 7 shows the chloride content increment along the rebar with respect to the uncracked conditions (ΔCl). This parameter was evaluated as follows:

$$\Delta Cl = Cl_{\perp cr,x} - Cl_{uncr,4} \quad (3)$$

where: $Cl_{\perp cr,x}$ is the chloride concentration at the depth x in the direction perpendicular to crack walls, while $Cl_{uncr,4}$ is the chloride content at the depth of about 41 mm (rebar depth) in uncracked conditions (average value of the two specimens of the same concrete type).

Results show that values of ΔCl are usually higher than zero, therefore the crack promoted the ingress of chlorides at rebar depth. ΔCl is on average higher for RC than for SFRC50. This could be ascribed either to higher crack widths in RC with respect to SFRC50 and/or to a different extent of debonding between concrete and steel rebar, that in RC specimens could have been higher and have promoted a higher penetration of chlorides.

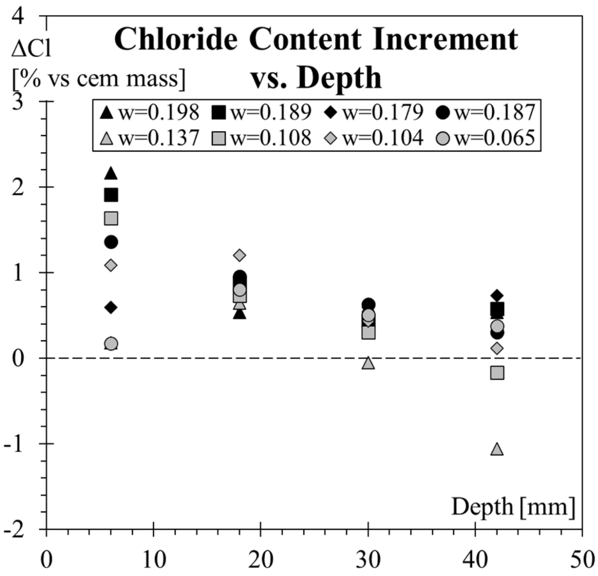

Figure 7: Chloride content increment in correspondence of the rebar due to the presence of the crack vs depth; black and grey symbols for RC and SFRC50, respectively, and crack width (*w*) in mm.

Finally, Figure 8 reports the values of chloride concentration at rebar depth in correspondence of crack walls, *i.e.* where corrosion initiated, as a function of pit depth (d_{pit}). In the previous work conducted on these specimens, no particular correlation was observed between pit depth and crack width [11], while from results shown in Figure 8, an increasing trend seems to correlate the pitting depth with the amount of chlorides where corrosion initiated. In the SFRC50 specimens, the cracks were on average smaller, and the damage along the reinforcement/concrete interface was expected to be more limited, leading to the ingress of a lower amount of chlorides.

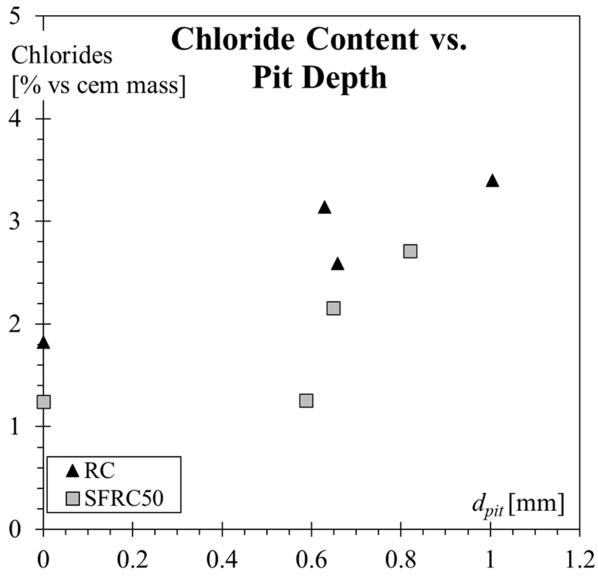

Figure 8: Chloride content in correspondence of the pit vs pit depth; black and grey symbols for RC and SFRC50, respectively.

However, of particular interest is the fact that both in uncracked concrete and some cases in correspondence of a crack (as can be seen also in Figure 4 and Figure 5), corrosion was not observed, even if chlorides were higher than the critical chloride threshold, as previously observed. This phenomenon could be explained considering macrocell, *i.e.* cathodic and anodic processes developing simultaneously in different areas of steel rebar. This may occur during a process of localized corrosion, promoting the anodic process in correspondence of pits where depassivation occurred, and localizing the cathodic process in the surrounding areas, enhancing passivity conditions. It has been reported that in a concrete showing low resistivity, and therefore allowing a discrete amount of current to flow through the electrolyte, the cathodic current can cover long distances (in the range of 1 m) to reach the local anode [1]. In the cracked concrete specimens, the crack accelerated the penetration of chlorides (most literature agrees on this [2,4,28]), and it is expected, even if it was not measured, that the critical chloride content was reached earlier in time in correspondence of cracks with respect to the uncracked zone, leading to the depassivation of steel. The corrosion initiation in those parts of the rebar could have protected the steel in uncracked concrete, even after the critical chloride content was reached. This could have occurred in both the RC and SFRC50 specimens, considering that adjacent cracks were quite close, 100 to 200 mm, and that concrete was often wet, leading to a low resistivity. The same explanation could apply to those cases where corrosion was not observed in correspondence of some cracks. In all the specimens where this case occurred, as already reported, the crack with no corrosion was adjacent to the one where the deepest pit was found. These pits could have been initiated earlier and developed with a higher corrosion rate, due to the formation of the macrocell, protecting the steel in the adjacent crack from corrosion.

3.3 Effects of corrosion on mechanical properties of steel

Table **2** summarizes the main experimental results of uniaxial tensile tests carried out on rebar segments. The pits studied are identified in Table 2 by crack number and letter by reference Figure 4 and Figure 5 for RC and SFRC50, respectively. Ultimate strain (ε_u) and ultimate load (F_u) are provided for all segments, while the load at reinforcement yielding (F_y) was reported only for one pit since the entire rebars extracted from concrete specimens were previously tested until failure as reported in Leporace-Guimil et al. [11]. Both yielding ($F_{y,th}$) and ultimate ($F_{u,th}$) load were predicted by assuming a circular residual cross-section (Figure 2a) as stated in the CONTECVET manual [29] and steel strengths (f_y and f_u) of the uncorroded bar. The latter assumption is in accordance to the recent results obtained by Chen et al. [10], in which no reduction of both f_y and f_u of corroded rebars was observed when the minimum remaining cross-section is considered. In particular, the following equations were used:

$$F_{y,th} = \frac{\pi\,(\phi_f)^2}{4}\,f_y \tag{4}$$

$$F_{u,th} = \frac{\pi\,(\phi_f)^2}{4}\,f_u = \frac{\pi\,[\phi_0(1-\Delta\phi)]^2}{4} f_u = A_0(1-\Delta\phi)^2 f_u \tag{5}$$

Table 2: Mechanical properties of rebar segments with pits located almost in the center.

Specimen	Crack	Letter	ε_u [-]	F_y [kN]	$F_{y,th}$ [kN]	$\frac{F_y}{F_{y,th}}$ [-]	F_u [kN]	$F_{u,th}$ [kN]	$\frac{F_u}{F_{u,th}}$ [-]
RC-5	1	B	0.0658	59.62	56.87	1.05	73.73	66.08	1.12
RC-5	2	-	0.0846	-	60.83	-	77.65	70.68	1.10
RC-5*	3	-	-	-	-	-	-	-	-
RC-5	4	B	0.0772	-	59.12	-	76.50	68.69	1.11
RC-6	1	B	0.0858	-	60.95	-	77.33	70.82	1.09
RC-6	2	B	0.0715	-	59.92	-	75.54	69.63	1.08
RC-6	3	A	0.0664	60.30	54.49	1.11	74.04	63.31	1.17
RC-6*	4	-	-	-	-	-	-	-	-
RC-7*	1	-	-	-	-	-	-	-	-
RC-7	2	B	0.0728	-	60.52	-	76.56	70.32	1.09
RC-7	3	B	0.0660	-	61.69	-	76.75	71.68	1.07
RC-7	4	-	0.0614	63.69	55.45	1.15	74.97	64.43	1.16
SFRC50-4	1	C	0.0811	-	61.89	-	75.93	71.92	1.06
SFRC50-4	2	A	0.0634	55.56	55.82	1.00	72.33	64.86	1.12
SFRC50-4	3	-	0.0950	-	65.31	-	78.34	75.88	1.03
SFRC50-4*	4	-	-	-	-	-	-	-	-
SFRC50-5*	1	B	-	-	-	-	-	-	-
SFRC50-5*	2	-	-	-	-	-	-	-	-
SFRC50-5	3	C	0.0818	-	60.46		78.37	70.25	1.12
SFRC50-5	4	A	0.0638	65.04	58.80	1.11	75.98	68.33	1.11
SFRC50-7	1	C	0.0854	-	57.67	-	77.68	67.01	1.16
SFRC50-7*	2	-	-	-	-	-	-	-	-
SFRC50-7	3	A	0.0706	62.33	58.15	1.07	75.50	67.57	1.12
SFRC50-7	4	A	0.0742	-	60.57	-	78.07	70.38	1.11

* The uniaxial tensile test was not carried due to the inadequate length of the bar

Figure 9 shows the ultimate strain (a) and load (b) vs. diameter loss for rebar segments affected by pitting corrosion. It can be clearly observed that pits, as already underlined in the literature [14], affects more ultimate strain as compared to the relative strength. For instance, a diameter loss of about 10% led to a strain reduction of about 25%, while the load reduction was around 5% (i.e. 5 times smaller). In addition, Figure 9 shows as this reduction is linear in the case of the load, while quadratic for the ultimate strain. Other Authors found a non-linear decrease of ductility with the reduction of the cross-section [10,12,15], even if one of the most known models to predict the decrease in ε_u in corroded rebars consider a linear reduction as a function of the percent reduction of bar cross-section [30]. This model was not applied against the present results since it requires an assumption on the value of percentage reduction of bar cross-section causing complete loss of ductility (which value can vary from 0.1 to 0.5), besides an accurate evaluation of the area reduction due to pitting. Comparing Figure 9a against Figure 9b, it can be also observed a higher variability of results in the case of ultimate strain, which led to a smaller value of R^2. Thus, it seems possible to consider a trend between ultimate strain and diameter loss, but mainly due to the high variability, further analysis and quantification are needed.

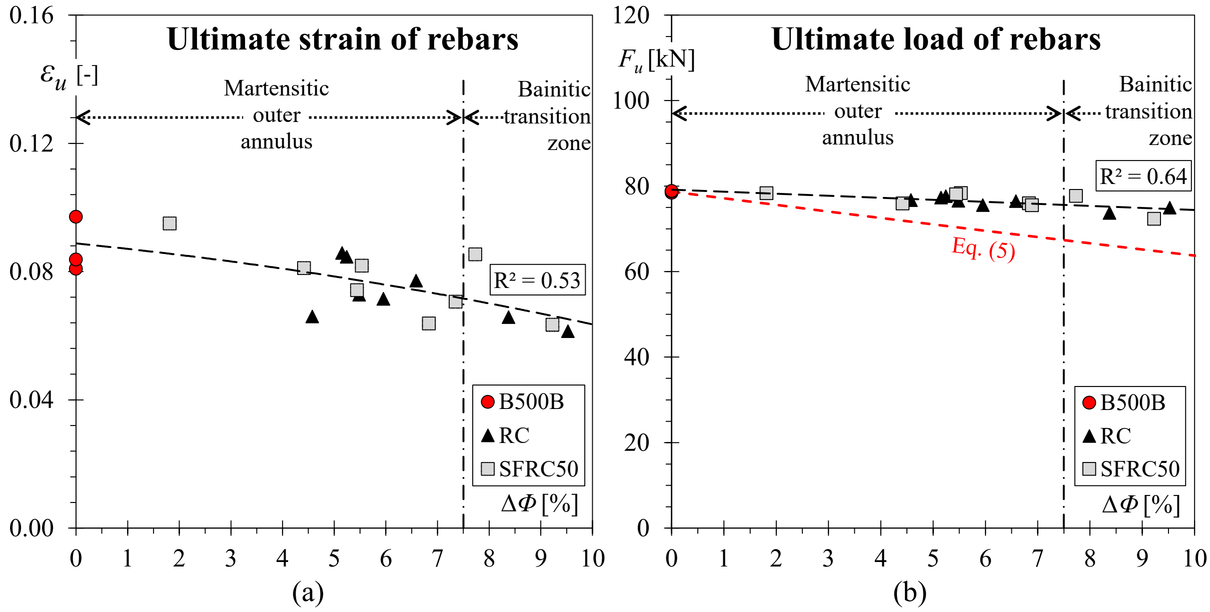

Figure 9: Ultimate strain (a) and ultimate load (b) vs diameter loss for rebar segments with pitting corrosion located almost in the center.

In the case of ultimate load, the experimental results were compared also against the provisions provided by Eq. 4. It can be observed that in the range of diameter loss considered (≤10%), Eq. 4 led to good and conservative prediction both in the case of F_y ($F_y/F_{y,th}$ equal to 1.08 in average, Table 2) and F_u ($F_y/F_{y,th}$ equal to 1.10 in average, Table 2 and Figure 9b), even if in the case of F_u the model seems to slightly increase its conservativeness with diameter loss increase. This underlines that the model prescribed by the CONTECVET [29] used with f_y and f_u of uncorroded bars is accurate and reliable. However, these results are related only to the martensitic outer annulus and in the first part of the bainitic transition zone. Thus, further research is needed in the case of higher diameter loss that provokes damage more in deep to affect also pearlitic/ferritic core.

4. CONCLUDING REMARKS

The mechanical behavior and the morphological characterization of corrosive attacks were investigated on rebars embedded in cracked reinforced concrete (RC) and Steel Fibers Reinforced Concrete (with 50 kg/m^3 of steel fibers, SFRC50) specimens in cracked stage, where corrosion initiated and propagated naturally during the exposure to wet and dry cycles for 280 days in a 5% NaCl solution. Based on the experimental results the following conclusion can be drawn:

(1) A morphological characterization of reinforcement was proposed by considering not only the pitting depth but also the different microstructural layers of rebars that were affected by chloride induced corrosion. In fact, the corrosion attack and the mechanical response of corroded rebars are also related to their microstructure.

(2) Corrosive attacks, presenting on average a quite shallow morphology, were observed in correspondence of almost all the cracks, whilst no corrosion was detected in the uncracked part of the specimens. Pits mostly involved the martensitic outer annulus and only in few cases the bainitic transition zone, never reaching the pearlitic/ferritic core. The diameter loss resulted included in the range of 1% to10%, being slightly higher for bars in RC specimens as compared to SFRC50 specimens.

(3) In SFRC50 specimens a lower amount of chlorides was observed in the direction perpendicular to crack walls, which was attributed to an increment of bond strength between rebar and concrete with respect to RC specimens. In the uncracked concrete a chloride content, similar among RC and SFRC50 specimens, higher than the critical

chloride threshold was measured. The formation of a microcell, between the anodic areas in correspondence of cracks and the surrounding areas, could have prevented the occurrence of corrosion far from cracks.

(4) To evaluate the yielding and ultimate load of corroded rebars, combining circular residual cross-section and f_y or f_u of uncorroded bars led to reliable and conservative predictions. However, the model seemed to slightly increase its conservativeness with diameter loss increase. A linear relationship seemed to be present between ultimate load and diameter loss as well.

(5) A weaker and more complicated relationship between ultimate strain and diameter loss was found as compared to the ultimate load. However, the results confirmed, once again, that pitting corrosion strongly reduces the ultimate strain of rebars as compared to the ultimate load.

ACKNOWLEDGMENTS

The Authors would like to deeply thank Prof. Giovanni Plizzari from the University of Brescia (Italy) for his precious suggestions in evaluating the effect of corrosion on RC and FRC structures.

REFERENCES

[1] Bertolini L, Elsener B, Pedeferri P, Redaelli E, Polder R. Corrosion of Steel in Concrete: Prevention, Diagnosis, Repair. Wiley-VCH. 2013.

[2] Gu C ping, Ye G, Sun W. A review of the chloride transport properties of cracked concrete: experiments and simulations. Journal of Zhejiang University: Science A 2015;16:81–92. https://doi.org/10.1631/jzus.A1400247.

[3] Käthler CB, Angst UM, Hornbostel K, Elsener B. Critical analysis of experiments on reinforcing bar corrosion in cracked concrete. ACI Materials Journal 2020;117:145–54. https://doi.org/10.14359/51722408.

[4] Russo N, Gastaldi M, Schiavi L, Strini A, Zanoni R, Lollini F. Effect of cracks on the service life of RC structures exposed to chlorides. fib International Conference on Concrete Sustainability, Acta Polytechnica CTU Proceedings; 2022, p. 511–7.

[5] Jaffer SJ, Hansson CM. The influence of cracks on chloride-induced corrosion of steel in ordinary Portland cement and high performance concretes subjected to different loading conditions. Corrosion Science 2008;50:3343–55. https://doi.org/10.1016/j.corsci.2008.09.018.

[6] Wang J, Nanukuttan S V., Basheer PAM, Bai Y. Influence of micro and macro cracks due to sustained loading on chloride-induced corrosion of reinforced concrete beams. Proceedings of the 4th International Conference on the Durability of Concrete Structures, ICDCS 2014 2014:1–9. https://doi.org/10.5703/1288284315481.

[7] Otieno MB, Alexander MG, Beushausen HD. Corrosion in cracked and uncracked concrete - influence of crack width, concrete quality and crack reopening. Magazine of Concrete Research 2010;62:393–404. https://doi.org/10.1680/macr.2010.62.6.393.

[8] Alarab LA, Ross BE, Poursaee A. Influence of Transverse Crack Opening Size on Chloride-Induced Corrosion of Steel Bars in Concrete. Journal of Bridge Engineering 2020;25:04020027. https://doi.org/10.1061/(asce)be.1943-5592.0001555.

[9] Chen E, Berrocal CG, Löfgren I, Lundgren K. Correlation between concrete cracks and corrosion characteristics of steel reinforcement in pre-cracked plain and fibre-reinforced concrete beams. Materials and Structures/Materiaux et Constructions 2020;53. https://doi.org/10.1617/s11527-020-01466-z.

[10] Chen E, Berrocal CG, Fernandez I, Löfgren I, Lundgren K. Assessment of the mechanical behaviour of reinforcement bars with localised pitting corrosion by Digital Image Correlation. Engineering Structures 2020;219:110936. https://doi.org/10.1016/j.engstruct.2020.110936.

[11] Leporace-Guimil B, Conforti A, Zerbino R, Plizzari GA. Chloride-induced corrosion in reinforced concrete and fiber reinforced concrete elements under tensile service loads. Cement and Concrete Composites 2021;124:104245. https://doi.org/10.1016/j.cemconcomp.2021.104245.

[12] Andrade C. Approach to the residual strength of steel bars due to corrosion. fib Capacity Assessment of Corroded Reinforced Concrete Structures CACRCS2021, 2021, p. 13–8.

[13] Almusallam AA. Effect of degree of corrosion on the properties of reinforcing steel bars. Constr Build Mater 2001;15:361–8. https://doi.org/10.1016/S0950-0618(01)00009-5.

[14] Cairns J, Plizzari GA, Du Y, Law DW, Franzoni C. Mechanical properties of corrosion-damaged reinforcement. ACI Materials Journal 2005;102:256–64.

[15] Andrade C, Alonso C, Garcia D, Rodriguez J. Remaining lifetime of reinforced concrete structures: Effect of corrosión on the mechanical properties of the steel. Life prediction of corrodible structures, Cambridge, UK: NACE; 1991, p. 12/1-12/11.

[16] Zhu W, François R, Poon CS, Dai JG. Influences of corrosion degree and corrosion morphology on the ductility of steel reinforcement. Construction and Building Materials 2017;148:297–306. https://doi.org/10.1016/j.conbuildmat.2017.05.079.

[17] Haefliger S, Kaufmann W. Influence of cross section loss on the stress-strain characteristics of corroded quenched and self-tempered reinforcing bars. Construction and Building Materials 2021;282:122598. https://doi.org/10.1016/j.conbuildmat.2021.122598.

[18] Ouglova A, Berthaud Y, Hild F, Bompard P, Foct F, Petre-Lazar I. Influence of corrosion on the mechanical behaviour of rebars in reinforced concrete structures. EUROCORR 2004 - European Corrosion Conference: Long Term Prediction and Modelling of Corrosion 2004.

[19] Tang F, Lin Z, Chen G, Yi W. Three-dimensional corrosion pit measurement and statistical mechanical degradation analysis of deformed steel bars subjected to accelerated corrosion. Constr Build Mater 2014;70:104–17. https://doi.org/10.1016/j.conbuildmat.2014.08.001.

[20] Zhang W, Zhang H, Gu X, Liu W. Structural behavior of corroded reinforced concrete beams under sustained loading. Constr Build Mater 2018;174:675–83. https://doi.org/10.1016/j.conbuildmat.2018.04.145.

[21] Imperatore S, Rinaldi Z, Drago C. Degradation relationships for the mechanical properties of corroded steel rebars. Constr Build Mater 2017;148:219–30. https://doi.org/10.1016/j.conbuildmat.2017.04.209.

[22] Moreno E, Cobo A, Palomo G, González MN. Mathematical models to predict the mechanical behavior of reinforcements depending on their degree of corrosion and the diameter of the rebars. Constr Build Mater 2014;61:156–63. https://doi.org/10.1016/j.conbuildmat.2014.03.003.

[23] Vanama RK, Ramakrishnan B. Improved degradation relations for the tensile properties of naturally and artificially corroded steel rebars. Constr Build Mater 2020;249. https://doi.org/10.1016/j.conbuildmat.2020.118706.

[24] Berrocal CG, Löfgren I, Lundgren K. The effect of fibres on steel bar corrosion and flexural behaviour of corroded RC beams. Engineering Structures 2018;163:409–25. https://doi.org/10.1016/j.engstruct.2018.02.068.

[25] François R, Khan I, Dang VH. Impact of corrosion on mechanical properties of steel embedded in 27-year-old corroded reinforced concrete beams. Materials and Structures/Materiaux et Constructions 2013;46:899–910. https://doi.org/10.1617/s11527-012-9941-z.

[26] Bautista A, Pomares JC, González MN, Velasco F. Influence of the microstructure of TMT reinforcing bars on their corrosion behavior in concrete with chlorides. Construction and Building Materials 2019;229:1–11. https://doi.org/10.1016/j.conbuildmat.2019.116899.

[27] Metelli G, Marchina E, Plizzari GA. Experimental study on staggered lapped bars in fiber reinforced concrete beams. Composite Structures 2017;179:655–64. https://doi.org/10.1016/j.compstruct.2017.07.069.

[28] Russo N, Gastaldi M, Marras P, Schiavi L, Strini A, Lollini F. Effects of load-induced micro-cracks on chloride penetration resistance in different types of concrete. Materials and Structures/Materiaux et Constructions 2020;53:1–14. https://doi.org/10.1617/s11527-020-01580-y.

[29] Rodriguez J, Arangocillo J, Andrade C, Izquierdo D. CONTECVET IN30902I - A validated Users Manual for assessing the residual service life of concrete structures. n.d.

[30] Coronelli D, Gambarova P. Structural Assessment of Corroded Reinforced Concrete Beams: Modeling Guidelines. Journal of Structural Engineering 2004;130:1214–24. https://doi.org/10.1061/(asce)0733-9445(2004)130:8(1214).

TABLES AND FIGURES

List of Tables:

List of Figures: